Polyacrylate-Graphene Oxide Nanocomposites for Biomedical Applications

Elison S. Ganya[1], Navneet Soin[2, Ψ,*], S. J. Moloi[1], James A. McLaughlin[2], W. F. Pong[3,*], Sekhar C. Ray[1,*]

[1] Department of Physics, College of Science, Engineering and Technology (CSET), University of South Africa, Private Bag X6, Florida, 1710, Johannesburg, South Africa.

[2] School of Engineering, Ulster University, Shore Road, Newtownabbey, Belfast BT37 0QB, Northern Ireland, United Kingdom.

[3] Department of Physics, Tamkang University, Tamsui 251, Taipei, Taiwan.

Abstract: Utilising a reverse micelle process, we have grafted polyacrylate (P) on graphene oxide (GO) to realise polyacrylate-graphene oxide (P-GO) nanocomposites, upon whose subsequent reduction, polyacrylate-reduced graphene oxide (P-rGO) nanocomposites are achieved. Using techniques such as ultra-violet photoelectron spectroscopy (UPS), X-ray photoelectron spectroscopy and X-ray absorption near edge structure (XANES) spectroscopy, in conjunction with high resolution microscopy, Raman spectroscopy and superconducting quantum interference device analysis, we have studied in-depth the electronic, microstructural, electrical and magnetic properties of these P-GO and P-rGO nanocomposites. While the polyacrylate grafting ensures a high solubility of the P-GO and P-rGO, the P-rGO nanocomposites additionally show a near doubling of the paramagnetic response (9.6×10^{-3} emu/g) as compared to the r-GO (5.6×10^{-3} emu/g) and P-GO (5.5×10^{-3} emu/g), respectively at 2 K. The grafting of diamagnetic polyacrylate enhances the magnetic response for the P-GO and P-rGO owing to the increase in the defect states, sp^3-type bonding and enhanced magnetic coupling between the magnetic moments arising due to the presence of nitrogen functionalities. This behaviour is further corroborated *via* the measurements of the electronic structure by XANES and UPS measurements. Thus, the possibility of manipulation of the magnetic behaviour along with the abundance of surface functional groups makes both P-GO and P-rGO nanocomposites highly conducive for deriving water-soluble functionalised graphene by linking affinity molecules with polyacrylate backbone for biological and bio-medical applications.

Keywords: Graphene Oxide; Polyacrylate; XANES; XPS**,** Magnetism

* Corresponding author(s): Raysc@unisa.ac.za (SCR), n.soin@ulster.ac.uk (NS) and wfpong@mail.tku.edu.tw (WFP)

I. Introduction

The sustained interest in graphene research has been triggered by its fundamentally intriguing mechanical, electrical, thermal and transport properties.[1-4] These properties uniquely qualify graphene for next-generation applications ranging from non-volatile memory devices[5], polymer nanocomposites[6], energy applications to bio-sensors[7], drug delivery[8], theranostics[9] and bioimaging such as magnetic resonance imaging (MRI)[10] among others. Especially for biological applications, graphene and its derivatives including graphene oxide (GO) and reduced graphene oxide (r-GO) have been functionalised with bio-active and bio-compatible polymers to generate stimuli-responsive materials which can then react to the local physiological environmental changes inside the body such as pH and temperature. On their own, both GO and r-GO have also been utilised as contrast agents in imaging techniques, however, due to their diamagnetic properties they have been side-lined as potential MRI contrast agents. The addition of magnetic nanoparticles results in enhanced signal, which improves the quality of the MRI, and thus colloidal iron oxides-based GO and r-GO composites including superparamagnetic iron oxide nanoparticles (SPIONs) have been reported. However, it has been observed that for the *in-vivo* applications, Fe_3O_4 nanoparticles tend to aggregate while the SPIONs can inhibit renal clearance leading to an accumulation of iron in the body, which not only affects the physiology but may also lead to negative MRI contrast[11-13].

Graphitic compounds generally show a diamagnetic response owing to the flow of current along their aromatic rings in the presence of applied external magnetic field.[14] However, more recently there has been a proliferation on the research of magnetism in carbon wherein ferromagnetic properties have been observed for graphitic compounds arising from the presence of defects, zig-zag edges and *via* hydrogenation, nitrogenation reactions.[14] While the magnetic properties of graphene for spintronic applications can be tuned *via* chemical functionalisation reaction, for bio-medical applications, the need for a bio-compatible surface is paramount. As outlined in our previous works, it is important to be able to manipulate the magnetic and electronic properties of graphitic compounds for various applications including spintronics and indeed MRI.[18] In literature, various polymers including polyethylene glycol (PEG),[15,16] polyacrylates[17,18] and block co-polymers of poly(ethylene oxide)–poly(propylene oxide)–poly(ethylene oxide)[19] have been utilised for GO/r-GO based biomedical applications. The motivation for grafting polyacrylate to GO/r-GO arises from our intent

to utilise it for solution-based applications of graphene. It is understood that the water dispersibility of graphene and r-GO owing to the lack of hydrophilic oxygen-groups is poor[20] and especially due to charge screening effects, the water-soluble GO tends to form aggregates in physiological buffers owing to the presence of ionic salts.[9] In the case of polyacrylate grafted GO/r-GO nano-composites, we have shown earlier ,good colloidal stability in physiological buffers such as phosphate buffer saline, (PBS, pH 6.0 - 9.0), 2-ethanesulfonic acid (MES) and carbonate.[18]

In the current work, we report on how the grafting alters the electronic and magnetic properties of the polyacrylate grafted GO (P-GO) and polyacrylate grafted reduced graphene oxide (P-rGO) composites. While in the first instance it can be assumed that owing to the diamagnetic nature of polyacrylate and indeed of GO/r-GO, a composite of the two materials should not show a significant magnetic response, however, we have observed an enhanced paramagnetic response from the composite. We have studied the variations in electronic and magnetic properties of the polyacrylate grafted GO/r-GO nanocomposites using techniques such as high-resolution transmission electron microscopy (HRTEM). Raman spectroscopy, X-ray diffraction (XRD), ultra-violet photoelectron spectroscopy (UPS), X-ray photoelectron spectroscopy (XPS) and superconducting quantum interference device (SQUID). The electronic structure of the nanocomposites was established using X-ray absorption near edge structure (XANES) spectroscopy. It was shown that for P-GO, P-rGO, the polyacrylate grafting creates defects sites and sp^3 type bonding, which may result in the enhancement of the paramagnetic properties. A combination of enhanced magnetic properties, biocompatibility and high colloidal stability with ample functional groups to further attachment of active drug molecules qualifies the P-GO/P-rGO nanocomposites for potential MRI application.

II. Experimental details

GO was prepared using the previously reported and well-established Hummer's method.[18,21] Briefly, 200 mg graphite powder, 100 mg $NaNO_3$ and ~5 mL H_2SO_4 were mixed together under vigorous stirring and cooled down to 0^{o}C. Next, 600 mg $KMnO_4$ was added to this solution in a controlled manner to ensure that the reaction temperature never exceed 20^{o}C. After the complete addition of $KMnO_4$, the solution was kept

stirring for another 30 mins and then ~10 mL water was added upon which the solution turned brownish yellow. This was followed by the addition of 500 mL of 3% H_2O_2 to reduce the residual permanganate. The obtained particles were thoroughly washed with warm water 7–8 times followed by air-drying and further dissolved in ~20 mL distilled water and centrifuged at 3000 rpm for 30 min. The supernatant was collected as GO solution and further utilised for polyacrylate coating.[18, 22]

The polyacrylate grafting of GO (P-GO) was carried out based on our previously reported reverse micelle medium process.[18, 22] Briefly, a concentrated aqueous solution of GO and acrylate monomers is dissolved in Igepal-cyclohexane reverse micelle to produce an optically clear solution and the polymerisation is initiated with persulfate in an oxygen-free atmosphere.[18] Upon the completion of polymerisation, the resulting particles were precipitated by addition of ethanol and then further washed with chloroform, ethanol and finally dispersed in water. Our previous extensive study has shown that 3-sulfopropyl methacrylate and its combination with polyethyleneglycol methacylate and N-(3-aminopropyl) methacrylamide works well in producing colloidally stable P-GO and as such has been used in this study as well.[18] For the production of polyacrylate grafted reduced GO, (P-rGO), 10 mL of the P-GO solution was taken in a glass vial and 1 mL hydrazine hydrate was added to it. The solution was then heated under stirring at 70 ^oC for 30 min during which time the solution slowly turned black, indicative of the reduction of GO. The ensuing solution was kept at room temperature overnight to ensure a complete reduction and was followed by dialysis process to remove the unreacted hydrazine. The dialyzed solution P-rGO was then used for further measurements.

The microstructural analysis of the synthesised polymer-graphene nanocomposites were performed using a Rigaku Smartlab X-ray diffractometer (Cu-$K\alpha$ line, 0.154 nm), Horiba scientific XploRA Raman microscope utilising a 532 nm (~2.41 eV) laser source, JEOL 2100 HRTEM. Surface chemical analysis comprising of XPS and UPS spectroscopy was carried out using a Kratos-Supra spectrometer equipped with monochromatic Al-$K\alpha$ ($h\nu$ = 1486.6 eV) and He-I ($h\nu$ = 21.22 eV) sources, respectively at base pressure 1.2 x 10^{-9} Torr at UNISA (Florida Science Campus). The XANES C *K*-edge, O *K*-edge and N *K*-edge surface measurements were performed at the Taiwan Light Source (TLS), Hsinchu, Taiwan in the

surface-sensitive electron-yield mode. For comparison between GO and P-GO, the XANES spectra were normalised to the edge jump (where the absorption coefficient reaches at a flat region above the edge) of unity.

Electrical sheet resistivity measurements by two probe method were carried out with the sample placed in the dark and at room temperature using Keithley 6487 Picoammeter with a built-in voltage source. The picoammeter was operated in the remote mode by connecting it to a personal computer through an RS-232 cable. An add-in utility for Microsoft Excel was installed in the computer for control of the picoammeter and for data acquisition. The current was measured with the voltage ranging from -1 to 1 V with a voltage step of 0.01 V with the current limit set to 2.5 mA. For these measurements, the synthesized GO/r-GO/P-rGO were dissolved into ethanol solution (0.1 mg/ml) and make them into thin film through drop casting method on a glass substrate (1.5 cm x 1.5 cm) and dried overnight at room temperature. The electrical contact between the probes and the dried films of similar size and thickens of ≈ 100 nm on the substrate was necessitated by drops of Ag-paste on the films. The thickness of the paste was enough to avoid scratching of the films since the probes have sharp ends. The separation between the probes was approximately 1.0 cm and was maintained throughout the measurements. Measurements were carried out at different points of the sample during set-up. The results were found to be very similar such that it can safely be assumed that for all samples the sheet resistance is independent of the different position.

The magnetic properties of the samples, on the other hand, were investigated using a superconducting quantum interference device (SQUID-type magnetometer with a sensitivity of $< 5\times10^{-8}$ emu.

III. Results and discussion

The TEM images of the r-GO and P-rGO are shown in Fig. 1(a, b), wherein the classical crumpled sheet-like morphology of the r-GO/P-rGO can be clearly observed. The TEM optical contrast observed for the r-GO arises from the possible stacking of layers during the hydrazine reduction process. In the case of P-rGO, the significant contrast observed in the middle of the image is from the polyacrylate coating which tends to be non-uniformly distributed and porous in nature.[18] For the XRD spectrum of the starting GO, as

shown in Fig. 1(c), a sharp C (002) peak with a full width half maxima (FWHM) of 2.32° was observed at ~12.6°, corresponding to an interlayer d-spacing of 0.702 nm.[21, 23] This enhanced d-spacing in GO, as compared to the graphite, is attributed to the heavy oxidation of the carbon lattice leading to the intercalation of water molecules and oxygen functional groups.[21, 23] These include hydroxyl, epoxide groups between the basal planes and carbonyl, carboxyl groups intercalated at the edge planes of the GO layers.[21, 23] Upon the hydrazine reduction, the r-GO exhibits a crystal structure closer to that of pristine graphite with the (002) peak position at ~23.8° (d-spacing = 0.374 nm), albeit with a large FWHM of ~13°, indicating a significant presence of defects in the r-GO.[21, 23] Upon the polyacrylate grafting of GO, a wide diffraction peak at ~21.8 and 22.8° corresponding to a d-spacing of 0.408 and 0.387 nm for P-GO and P-rGO, respectively, was observed. This slightly higher value of d-spacing for P-GO and P-rGO can be ascribed to not only the presence of oxygen containing surface functional groups but also the presence of defects and polyacrylate coating on the graphene oxide sheets and is in accordance with our previously published work.[18, 22]

For carbon nanomaterials, Raman spectroscopy is the most commonly used assessment tool for probing the electronic structure, crystallinity and the presence of defects.[24-26] As seen in Table 1 and Fig. 1(d), the conversion of pristine graphite to GO leads to significant changes in the band intensities. In the first-order Raman spectra, the sp^2 carbon related G-mode at ~ 1580 cm^{-1}, arises from the doubly degenerate TO and LO phonon mode (E_{2g} symmetry) at the Brillouin zone centre, while the D-mode at ~1350 cm^{-1} arises due to the breathing-like modes (corresponding to TO phonons close to the K point) activated by defects including substitutional heteroatoms, grain boundaries, respectively.[24,25] Additionally, the fitting of the Raman spectra required two additional bands at ~1610 cm^{-1} (D` band) which occurs *via* an intra-valley double resonance process in defective carbon materials and an another peak for the D**-band at ~1500 cm^{-1}.[25] The D** peak has been argued to arise either from the contribution of the finite sized graphitic crystals, sp^3 C-H vibrations or *via* a combination of the C=C stretching and CH wagging modes of trans-polyacetylene.[26-28] It is known that during the oxidation process, the graphitic sheets are not only exfoliated but also break down into smaller sizes and as such for GO, the D-band intensity (I_D/I_G 1.12 *vs*. 0.2 for graphite) and its FWHM (128 cm^{-1} *vs* 57 cm^{-1} for graphite) related to the defects and edge density is

understandably significantly enhanced.[21,23] The higher intensity broad D-band, higher I_D/I_G ratio for GO and blue shift (≈15 cm^{-1}) of the G-band confirms the structural changes including introduction of sp^3-type defects and oxygen groups in the carbon lattice. For P-GO, the apparent G-band is broadened and shifted to higher wavenumbers owing to the structural defects and attachment of oxygen moieties from polyacrylate coating. However, upon its reduction to P-rGO, a significant reduction in the G-band FWHM was observed with an increase in the I_D/I_G ratio (~1.35) which is suggestive of a reduction in the average sp^2 domain size upon hydrazine treatment with the new graphitic domains of a smaller size than that of GO.[22, 25] It should be noted that during the whole process of the conversion of graphite to GO and subsequent grafting of polyacrylate, the area under and the intensity of the D**-band kept increasing which can be correlated to the finite crystallite size and defect density.[18, 22]

Figure 2(a) displays the high-resolution C 1*s* core level XPS spectra of the pristine GO, r-GO, P-GO and P-rGO. The peak fitting analysis was performed using Gaussian line shapes and to the following peak component assignments: C-C/C-H at 284.5/285.0 eV (peak C1), C-OH group with a chemical shift of +1.5 eV (285.9 - 287.0 eV, peak C2), C=O groups with a shift of +2.5 eV (286.9 – 287.5 eV, peak C3) and O=C-OH with a chemical shift of +4.0 eV (288.4 – 289.0 eV, peak C4), respectively.[22, 29] The C 1*s* XPS spectrum of starting GO is indicative of the high degree of oxidation with the characteristic peaks observed at ~285.0, 286.5 eV, 288.4, 292.9 and 295.6 eV corresponding to C-C/C-H, C-OH, C=O, O=C-OH and π-π* shake up satellite, respectively.[18,22,29] It should be noted that various structural models of GO include an epoxide group (C-O-C) which has a binding energy similar to that of C-OH, however its precise contribution is difficult to ascertain. In their work on the thermal deoxygenation of GO, Sharma *et al*.[23] have attributed the component at ~286.5 eV to the C-O-C group with the smaller components at ~ 287.5 and 288.9 eV being ascribed to carbonyl (>C=O) and carboxyl groups (O=C-OH). It should be noted that for the P-GO, a small amount of nitrogen (see Table 1) is also incorporated into the carbon lattice with possible components of C=N bonds at ~286.5 eV, however, its individual contribution was not ascertained.[22] To characterise the degree of oxidation in GO, we have looked at the area excluded by the sp^2 carbon fraction, which was estimated by dividing the area under the sp^2 peak with that of the total C 1s peak area. It should be noted that carbon atoms associated with hydroxyl and epoxy groups are sp^3

hybridised and hence is a good indicator of the oxidation levels. For GO, this sp^2 fraction was calculated to be ~50% thereby further confirming the heavy oxidation commonly observed in Hummer's method.[23] Owing to the increase in the amount of the polar oxygen groups, the C 1*s* peak becomes more asymmetric and broadens towards the high binding energy side.[29] This trend is clearly observed as the graphite is converted to GO (as discussed above) and for the P-GO as well.[29] Furthermore, upon the grafting of polyacrylate on GO, the C 1*s* peak of of P-GO broadened further (Fig. 2(a)), which can be attributed to the relative increase of contributions from the carbon-oxygen double bonds (C3+C4 components from ~11% to 16%) and the reduction in the carbon-oxygen single bonds (C2 component from ~38% to 30%) with respect to the graphitic sp^2 and hydrogen-bonded carbon (C1 component) in GO samples (see Table 2). These results are in accordance with our earlier reports[18, 22] and more recently of Consiglio *et al*.[29]

We have also considered the O 1*s* core level spectra of the GO, r-GO and P-rGO and have deconvoluted it into multiple components. For the GO, the O 1*s* spectra displayed four components at 531.3 (O1), 531.9 (O2), 532.8 (O3) and 534.4 eV (O4) corresponding to C=O, C-O, O=C-OH and intercalated water, respectively.[18,22,29] Upon reduction (see Table 1 and Table 2), the r-GO showed a marked reduction in the peak O3 corresponding to the COOH groups, which are known to be the most prone to reduction in GO.[21,23] Now, upon grafting, the P-GO again displayed a slight change in the symmetry in the high binding energy side and components were observed at 530.4, 531.8, 532.7 and 536.2 eV, corresponding to C=O, C-O, O=C-OH/C-OH and chemisorbed water and/or O_2, respectively.[18, 22] Similar to the variation of the contribution from double bonded C=O in the C 1*s* spectra, both the P-GO and P-rGO exhibits a relative increase in the contribution assigned to the carbonyl (C=O) and hydroxyl (C-OH) components (~532.0 eV, peak O2) with respect to the single bonded (C-O) component and is in accordance with those reported by Consiglio *et al*.[29] It should be noted that there could be some contribution from the oxides of nitrogen for the peak at ~532.0 eV, however their individual contribution could not be ascertained.[22] Using the areas under the peaks for various components, a quantitative analysis show that for GO, an overall ratio (C2+C3+C4)/C1 *i.e.* ratio of the oxygen-containing groups to graphitic carbon (sp^2) and hydrogen-bonded carbon, of 1.07 is calculated, which is comparable to other reported instances of GO films.[30] Upon polyacrylate grafting, a reduction in this ratio is observed along with a relative increase in the (O2+O3)/O4

ratio (see Table 2), which all points towards an increase in the C=O and OH groups with respect to the C-O bonds associated with polyacrylate coating.[29] Considering the N 1*s* core level spectra, while no nitrogen was observed for the GO; a clear distinction was observed between the r-GO and polyacrylate grafted P-GO & P-rGO nanocomposites. The N 1*s* spectra of r-GO was deconvoluted into two peaks at 399.9 eV and 401.9 eV, corresponding to pyrrolic and graphitic nitrogen, respectively.[18, 22, 31, 32] For the P-GO and P-rGO, additional peak at ~398.2 eV is assigned to the sp^2 hybridised aromatic N corresponding to amine/pyridinic nitrogen and ~402.6 eV to quaternary nitrogen respectively.[31,32] These primary amine groups on the polyacrylate backbone are also responsible for the lowering of the surface charge of the P-GO and P-rGO as reported in our earlier works.[18] The role of these nitrogen functional groups in altering the magnetic behaviour of the P-GO/P-rGO will be discussed in later sections.

In general, for carbon materials, the XANES spectra can be largely divided into three regions: π* resonance (285±1 eV), C-H* resonance (288±1 eV) and a broad region between 290–315 eV, corresponding to σ* resonance.[23, 31-33] For the starting GO, the C *K*-edge XANES spectra shown in Fig. 3 (a, b) clearly shows that despite the significant oxidation (~50 at.%), the aromaticity of the graphitic structure is still maintained, as shown by the presence of unoccupied π* states (1s→π*) at ~285 eV and σ* states (1s→σ*) at 291.0 eV, respectively.[23, 34] For the pristine GO, absorption features were observed at 283.7, 285.4, 287.8 and 290.5 eV. The sharp feature at 283.7 eV has been previously ascribed to the presence of surface defects, dangling bonds and low-crystallinity carbon.[35] It should be noted that this feature was only observed for the GO and r-GO and disappeared upon the polyacrylate grafting and thus points towards a high possibility of saturation of the dangling bonds on GO by polyacrylate. The other features for GO at ~285.4 eV are ascribed to C=C bonds at 287.8 eV to π* C-O-C/C-OH and at 290.5 eV to π* C=O-OH/C=O groups, respectively arising from the oxidation of the graphite lattice.[32, 34, 36] The σ* resonance attributed to single-bonded oxygen (C-O) at 297.5 eV as well as the C=O σ* feature from carboxyl at around 303 eV were observed, however, owing to the high functionalisation and interference they could not be well resolved. Upon the reduction of the GO → r-GO, the feature at ~283.7 eV is downshifted to ~283.2 eV while its relative intensity is increased, which may correspond to the increase in the surface defects and is corroborated by Raman analysis where an increase in the I_D/I_G ratio was observed. Similarly, as compared to GO, the r-GO, all the other features in the π* region

were downshifted by ~0.4 – 0.5 eV and such shift has been observed in our previous work as well.[37] Particularly, the downshift and reduction in the intensity of the previously observed (for GO) mixed hydroxylated (C-OH) and ether-linked carbon species (C-O-C) at 287.8 eV indicates clearly that the hydroxylated species are removed during the reduction process by hydrazine hydrate, leading to the alteration of the electronic structure of the r-GO.[34,38] Now, due to the presence of electronegative oxygen, the hydroxyl groups bonded to the carbonyl carbon see an upshift in their π* position.[34, 39] The removal of these hydroxyl groups therefore leads to a reduction in the electronegative oxygen content thereby leading to a reduction in the π* resonance positions and is consistent with the results reported by Urquhart *et al*.[39] in their computational work. Now, upon the grafting of polyacrylate on GO (P-GO), weak features at ~284.2, 287.8 eV (π* C-O-C/C-OH) were observed with other relatively stronger features at 284.9 (C=C), 286.7 (π* C-O) and 290.7 eV (π* C=O-OH/C=O), respectively. Considering the intensities of the features at 286.7 eV and 290.7 eV for the P-GO and comparing them to the peak intensities of the corresponding features for GO, a relative increase in the contribution from the C=O and a reduction in the C-O bonds can be observed. Indeed, this trend was ascertained from the C 1*s* XPS analysis as well and therefore provides further evidence of the successful grafting of the polyacrylate on GO. In the case of P-rGO, strong absorption features were observed at ~285.0 (C=C), 286.5 (π* C-O), 287.2 (π* C-O-C/C-OH) and 290.7 eV (π* C=O-OH/C=O), along with some weaker features at 294.7(σ* C-C) and 297.6 eV (σ* C-O), respectively.[36-40] The deconvolution parameters including peak position, intensity and FWHM values are summarised in Table 3.

The O *K*-edge XANES spectra is shown in Fig. 3(c, d). For the GO, in the π* region, two absorption features were observed at ~528.9 and 529.6 eV and further deconvoluted using Gaussian components (see Table 4). These absorption features are ascribed to the corresponding π* resonances from carbonyl (C=O) and carboxylic (COOH) groups, respectively.[34, 39] The shoulder at 535 eV is a hydroxyl (O-H) derived σ* state, while the σ* features attributed to single bonded oxygen groups such as hydroxyl (C-OH) and epoxide (C-O-C) which have been shown to provide a broad feature at ~537 eV can also be observed.[34,39] The C=O σ* intensity which should be present at ~539 eV, however, could not be well resolved but both the C *K*-edge and O *K*-edge spectra are consistent with other published reports on GO. Upon reduction, the O *K*-edge XANES spectra of r-GO showed a clear reduction in the intensity and area of the peak associated with the π* (C=O-

OH) resonance. This behaviour is associated with the ease of removal of the COOH groups in the GO structure and has been reported earlier as well.[23] Importantly, the ratio of intensities of π* excitation of oxygen in the sp^2 network to that of σ* resonance around 536 eV is representative of the oxidation and indeed the sp^2 content. As compared to GO (0.39), an increase in the intensity of sp^2-derived unoccupied π* resonance is observed for the r-GO (0.45) suggestive of restoration of the π conjugated network upon reduction.[38] As expected, for the P-GO, this ratio remains rather low (0.35) owing to the significant disruption of the sp^2 states but is improved (0.46) for the P-rGO. It should be noted that the enhanced electronegative oxygen content upon the polyacrylate grafting of GO, leads to a significant shift in the π* resonance peak to ~530.6 eV (for P-GO) and ~530.4 eV (for P-rGO) as compared to a value of ~529.8 eV for GO.[39] For both the polyacrylate grafted P-GO and P-rGO, deconvoluted peaks were observed at ~530.0 and 530.7 eV corresponding to $1s \rightarrow \pi^*$ (C=O)[32] excitation and oxygen in the -OH groups, respectively and is line with the earlier discussed XPS measurements.[41]

Fig. 3(e, f) shows the N *K*-edge XANES spectra wherein the intensity of the main π* peak reflects the nitrogen content due to the delocalisation of the π* states with N $2p_z$ orbital components providing much smaller transition dipole moment values between the N 1*s* orbitals.[31, 32] Indeed, for the low nitrogen content of the r-GO and P-GO, the π * region is relatively noisy as compared to the P-rGO, which provides a strong absorption feature at ~398 eV. In the σ* region, the observed strong $1s \rightarrow \sigma^*$ transition at ~405 eV is associated with the superposition of graphite-like and pyridine-like nitrogen structures and/or photoionization of the N 1s electrons.[31, 32] The π* region of the N *K*-edge spectrum was deconvoluted into multiple components using Gaussian line shapes reflecting the spectral evidence for the local electronic states bound to the nitrogen sites. For the r-GO, the spectrum showed two components at ~398.9 and 399.8 eV corresponding to pyridine-like (N-6) bonding and pyrrole (N-5) like bonding, respectively. Similar peak positions have been reported by Soin *et al*.[31] and Geng *et al*.[35] in their work on nitrogen doping of graphene. For the P-GO, a small upshift in the peak positions was observed with peaks at 399.3 and 400.2 eV, which could be ascribed to the effect of polyacrylate grafting. In the case of P-rGO, peaks at 397.0, 397.5 and 398.5 eV corresponding to nitrogen in nitride (C=N) phase, pyridine-like bonding and pyrrolic/substitutional graphite like bonding, respectively were observed.[32] With the increase in the nitrogen content, the intensity of the feature associated with the non-

graphitic type structures *i.e.* pyridinic nitrogen increases while that of the substitutional graphene-like structures reduces which leads to an increase in the defect structures and is supported by the increase in the I_D/I_G ratio (Table 1).[32]

For the electrical measurements, the linear current-voltage (I-V) relationship for the GO/r-GO/P-rGO were obtained (Fig. 4(a, c, e)) by sweeping the voltage in the sequence 0 → +1 → 0 → -1 → 0 V using a step voltage of 0.01 V. As expected, the GO showed poor conductivity and highly insulating behaviour owing to the heavy oxidation of the carbon lattice. With the subsequent removal of oxygen functional groups and an increase in the sp^2 content of the films (as confirmed by XANES and Raman spectroscopy), the r-GO films showed a significantly enhanced (~10^6 times higher) current response. The grafting of polyacrylate, a non-conducting polymer, onto GO (P-GO) leads to lower (~10^4 times than r-GO) current response owing to the extended polymer chains hindering the charge flow as well as the higher sp^3 content (see Table 1). However, P-rGO current response is nearly ~10^2 higher than that of GO, albeit still lower than the r-GO, which can be attributed to the lower amount of oxygen functional groups.[37] The corresponding log I-V curves for the GO/r-GO/P-rGO are shown in Fig. 4(b, d, f) in which the GO shows a symmetric log I–V curve which have a small hysteresis loop on the positive voltage side and ranges between 0 V to 0.5 V, while the P-rGO displayed a small hysteresis loop on the positive voltage side in the range 0.25-0.75 V. The hysteresis effects usually arise from deeply trapped charges due to the presence of defects in the P-GO as the escape time for the trapped charges is longer than the time it takes to make the semi-log sweep.[42] From the above measurements, we have obtained the sheet resistances of GO, r-GO and P-rGO are 4 x 10^9 Ω/sq, 2.5 x 10^3 Ω/sq, and 3.3 x 10^7 Ω/sq, respectively that are comparable with the reported values.[43]

The observed changes in the electrical properties are further supported by the surface sensitive UPS He-I (hν = 21.22 eV) measurements as the high photon flux source is only able to excite the valence band electrons and thus has been used to probe the position of the Fermi energy (E_F) with respect to the vacuum level.[37,44] The UPS He-I spectra consists of two areas of significant interest: the low binding energy region where the valence band maximum (VBM) relative to the E_F can be determined and the high binding energy where the electrons are able to overcome the work function (Φ) of the material.[44] The Φ itself is determined by subtracting the

width of the spectrum (energy difference between the E_F and the high binding energy cut-off) from the He-I excitation energy (21.22 eV).[45, 46] Accordingly, the secondary electron threshold energies for the r-GO (17.3 eV), P-GO (17.4 eV) and P-rGO (17.7 eV) are shown in Fig. 2(d). The VBM position of 4.0 eV for r-GO is further shifted to 4.1 and 4.2 eV for P-GO and P-rGO indicative of a reduction in the density of states (DOS) at/near VBM or E_F with the polyacrylate grafting. This is expected as polyacrylate is not expected to contribute significantly to the C 2pπ states and enhance the DOS. The Φ for the r-GO, P-GO and P-rGO, using the threshold energy, has been estimated to be ~4.0 eV, ~3.9 eV and ~3.8 eV, respectively. The reduction in the (Φ) of r-GO to 4.0 eV, as compared to GO (Φ ~5.0 eV owing to surface dipole moments of oxygen functional groups disrupting the π-conjugation) is understandable in terms of the removal of oxygen functional groups and a consequential increase in the sp^2 content.[37,44] In general, the surface functional groups and the electronic structure of the material are thought to be the most important factors which affect the Φ.[44,47] In the case of P-GO and P-rGO, while the overall oxygen content is increasing and the area under the C *K*-edge π*-peak (incorporating sp^2 bonds) is reducing (P-rGO (2.05 a.u.), P-GO (1.25 a.u.) *vs.* 2.3 a.u. for r-GO), the Φ is still being reduced marginally. To account for this, it should be noted that the incorporation of nitrogen too is taking place simultaneously for both P-GO and P-rG, which has the opposite effect of oxygen and introduces extra π electrons near the E_F due to the formation of N lone-pair electrons, π electrons of C-N bonds thereby reducing the Φ.[31, 32] Now, this variation of the VBM and Φ implies a change in the dipole moment affecting the charge redistribution and consequently influences the magnetic behaviour of P-rGO.[37] It has been reported earlier from first-principle calculations that changes in magnetic behaviour can be attributed to introduction of defects which causes a shift in the quasi-localised states at the Fermi level.[37, 48] Invariably, the N introduction also leads to an increase in the defect density which play a role in the change of magnetic properties and is discussed further.

The measured magnetic behaviour *via* M-H hysteresis loops at 2K and M-T loops at 500 Oe are shown in Fig. 4(g) & 4(h), respectively. A weak paramagnetic behaviour was observed for GO with a saturation magnetisation (M_S) of 4.6 $\times 10^{-3}$ emu/g and 5.6 $\times$ 10^{-3} emu/g for the r-GO, respectively with low coercive field values (H_C). For both GO and r-GO, the observed magnetic behaviour arises due to the contributions

from defects and the non-bonding π-electron states localised at the graphene layer edges *i.e*. dangling bonds at the edge planes, as corroborated by the XANES measurements.[48-50] For both case, a variety of defects including topological defects, vacancies, adatoms, wrinkles, corrugations *etc*. besides the binding of oxygen atoms to the carbon lattice can give rise to magnetic moment. [48-50] In the case of GO, the hydroxyl group bonded to C-atom of the sub-lattice too can induce local magnetic moment. In fact, Wang *et al*.[51] have shown that a magnetic moment of 1.2 μ_B is developed in the case when a hexagonal graphene ring is bonded to two hydroxyl groups. Such magnetic moment developed due to oxygen moieties should be considered along with the defect induced magnetic moment for the total magnetic behaviour of GO. Extensive literature reports suggest that the not only the deoxygenation itself but its underlying process *i.e*. hydrazine[52], thermal[53] or Birch[54] reduction strongly influences the magnetic properties of the resulting r-GO. In our case, the strong reducing agent, hydrazine hydrate, introduces significant defects and nitrogen dopants into the r-GO graphitic lattice which generates localised magnetic moment.[52] It has been argued earlier as well that as compared to GO reduced in a hydrogen environment, the use of ammonia (nitrogen) conditions leads to the oxygen concentration being more efficiently reduced with simultaneous introduction of N-defects leading to higher magnetization.[55] It has also been shown by Taniguchi *et al*.[56] that localized electronic states in r-GO also add spin moments to the sp^2 nanodomains which result in singly occupied molecular orbital levels in the π- π* gap leading to the emergence of magnetism. For both GO and r-GO, an increase in the magnetisation with the reduction of temperature was observed owing to the ease of the alignment of magnetic spins at low temperatures (2 K). However, for both the GO and r-GO as the magnetic moments are not coupled, only weak paramagnetism is observed (M_S of 4.6×10^{-3} and 5.6×10^{-3} emu/g for GO and r-GO, respectively. However, had the magnetic moments been coupled by long-range interactions, ferromagnetic, anti-ferromagnetic or super-paramagnetic behaviour should have been observed. For GO, the measured values are similar to those reported by Qin *et al*.[55]

The grafting of diamagnetic polyacrylate on its own is not expected to enhance the magnetic response of the composites and indeed the maximum magnetisation of the P-GO (M_S of 5.5×10^{-3} emu/g) is very similar to that of the r-GO. However, upon the reduction of the P-GO to P-rGO, a near doubling of the M_S value to 9.6 $\times 10^{-3}$ emu/g was observed. Furthermore, considering the P-rGO, the saturation magnetic moment was found

to be 2.79 × 10^{-3} emu/g with a remnant magnetisation value of 8.6 x 10^{-6} with a coercivity value of nearly 12 Oe. As mentioned earlier, despite their suitable applications in bioimaging, the lack of magnetic moment renders pristine GO unsuitable for MRI applications. However, the possibility of improving its magnetic response by introducing defects or manipulating oxygen functionalities renders it an excellent candidate for MRI contrast agents.[57] In their work, Enayati *et al.* reported on the variation of the magnetic properties of GO produced by strong and weak oxidising agents which were then further exposed to 1.23 MeV γ-rays. It was observed that as compared to w-GO (Ms 0.013 emu/g), the s-GO showed higher magnetisation (Ms 0.023 emu/g) which was further expressed upon its reduction (Ms 0.033 emu/g).[57] Furthering their work, the irradiated samples were further annealed at various temperatures (200-800 ^{o}C) to enhance their magnetism. It was observed that at 600 ^{o}C, the saturation magnetisation not only reached a maximum value of nearly 0.16 emu/g but the r-GO samples showed no toxicity when measured using an MTT ((3(4-(4,5-dimethylthiazol-2-yl)-2,5-diphenyl-tetrazolium bromide)) assay and as such has been proposed as an alternative MRI contrast agent.[57, 58]

Considering the GO's prepared in this work, as the GO itself is non-stoichiometric, consequently the resulting P-rGO system too is chemically quite complex, where it includes a variety of oxygen, nitrogen surface moieties and topological, adatoms and structural defects, all of which can contribute to the magnetic moment. In terms of the defects, it has been previously reported by He *et al.*[59] that the magnetisation of HOPG is closely correlated to the defect density with an almost linear relationship observed between the I_D/I_G ratio and magnetisation. Indeed, the P-rGO shows the highest defect density value (see Table 1). Considering this along with the quantification from the XPS analysis, the P-rGO shows the highest nitrogen content (~1.9 at%) and as such highest magnetisation is expected arising due to the extra π-electron from nitrogen making the structure electron-rich, thereby, enhancing the magnetic coupling between magnetic moments.[31, 32, 52] However, there is an on-going debate in terms of the effect of the various nitrogen functional groups especially the pyrrolic and pyridinic nitrogen moieties and how they affect the magnetisation of graphene. While, Ito *et al.*[60] have observed that the presence of pyrrolic groups lead to a reduction in the magnetisation values, Miao *et al.*[61] have observed enhanced ferromagnetism in N-doped graphene with high pyrrolic content which was shown to induce a net magnetic moment of 0.95 μB/N atom. Theoretical calculations also reveal that graphitic

N does not contribute to the magnetism in graphene and in the case where there are paired defects such as graphitic-graphitic, graphitic-pyrrolic and graphitic-pyridinic N pairs, the system prefers a non-magnetic state.[62] Simultaneously, it was shows that pyrrolic nitrogen in the carbon lattice becomes more stable when the defect site is bonded to hydroxyl or carbonyl groups.[62] Considering the Raman spectra of Fig. 1 and the XPS analysis (Fig. 2), a small amount of pyrrolic nitrogen was only observed in the case of P-GO and P-rGO which had a higher defect ratio and amount of carbonyl groups. Density function theory calculations have shown that when pyridinic nitrogen is bonded to oxygen, then the system becomes spin-polarised with a magnetic moment of 0.56 μB.[62] Considering that the P-rGO still contains a considerable amount of oxygen (20 at%), there is a high possibility that the pyridinic nitrogen can interact with some of the oxygen groups either in the r-GO lattice or indeed in the polyacrylate itself or that the magnetic behaviour is more expressed due to the parallel spin orientation between the nitrogen and oxygen radicals, especially at low temperatures.[63] Thus, the enhanced magnetisation in P-rGO can be ascribed to high defect density, N-doping and enhanced magnetic coupling between the magnetic moments. We believe that the possibility of manipulation of this magnetic behaviour along with the abundance of surface functional groups makes both P-GO and P-rGO highly conducive for deriving water-soluble functionalised graphene by linking affinity molecules with polyacrylate backbone for future biological and bio-medical applications.

IV. Conclusions

In a summary, we have synthesized polyacrylate grafted graphene oxide (P-GO) and polyacrylate grafted reduced graphene oxide (P-rGO) nanocomposites using a reverse micelle medium process. A comparison of peak intensities of the specific C=O and C-O bonds corresponding to polyacrylate in the XPS and XANES spectra provide evidence of successful grafting of polyacrylate on GO. While the polyacrylate grafting saturated the dangling bonds on the GO and r-GO surfaces, it also resulted in the formation of defects as evident by the Raman analysis. Furthermore, a relative reduction in the normalised π* intensity for XANES spectra implied a decrease in the sp^2 content for P-GO and P-rGO samples, which is consistent with the observed increase in the I_D/I_G ratio obtained from the Raman spectra indicating an introduction of the sp^3-type defects. The presence of nitrogen groups arising from the polyacrylate grafting resulted in a lower work

function and a higher conductivity of the P-rGO with the highest magnetisation value of 9.6×10^{-3} emu/g (at 2 K) amongst all samples. This enhanced magnetisation was attributed to the high defect density and N-doping arising from the polyacrylate grafting which can be further manipulated to change the magnetic behaviour of the nanocomposites. It is envisaged that for the water soluble P-GO and P-rGO, the combination of abundant surface functional groups allowing the attachment of drug-molecules in conjunction with the enhanced magnetic response will lead to targeted drug delivery and magnetic contrast bio-medical imaging applications.

Acknowledgements

N.S. and S.C.R. gratefully acknowledge the financial support received from the National Research Foundation (NRF), South Africa (Grant Nos. ECR180426324617 and EQP13091742446).

The authors declare no conflict of interest.

References

[1] D.A. Dikin, S. Stankovich, E.J. Zimney, R.D. Piner, G.H.B. Dommett, G. Evmenenko, S.T. Nguyen, and R.S. Ruoff, "Preparation and characterization of graphene oxide paper," Nature **448**, 457 (2007).

[2] C. Gómez-Navarro, R.T. Weitz, A.M. Bittner, M. Scolari, A. Mews, M. Burghard, and K. Kern, "Electronic transport properties of individual chemically reduced graphene oxide sheets," Nano Lett. **7**, 3499 (2007).

[3] Y. Zhang, Y.-W. Tan, H.L. Stormer, and P. Kim, "Experimental Observation of Quantum Hall Effect and Berry's Phase in Graphene," Nature **438**, 201 (2005).

[4] H. Kim, Y. Miura, and C.W. Macosko, "Graphene/Polyurethane Nanocomposites for Improved Gas Barrier and Electrical Conductivity," Chem. Mater. **22**, 3441 (2010).

[5] H.Y. Jeong, J.Y. Kim, J.W. Kim, J.O. Hwang, J.-E. Kim, J.Y. Lee, T.H. Yoon, B.J. Cho, S.O. Kim, and R.S. Ruoff, "Graphene oxide thin films for flexible nonvolatile memory applications," Nano Lett. **10**, 4381 (2010).

[6] G. Mittal, V. Dhand, K.Y. Rhee, S.-J. Park, and W.R. Lee, "A review on carbon nanotubes and graphene as fillers in reinforced polymer nanocomposites," Journal of Industrial and Engineering Chemistry **21**, 11 (2015).

[7] S. Cinti and F. Arduini, "Graphene-based screen-printed electrochemical (bio)sensors and their applications: Efforts and criticisms," Biosensors and Bioelectronics **89**, 107 (2017).

[8] S.E. Matthews, C.W. Pouton, and M.D. Threadgill, "Macromolecular systems for chemotherapy and magnetic resonance imaging," Advanced Drug Delivery Reviews **18**, 219 (1996).

[9] K. Yang, L. Feng, X. Shi, and Z. Liu, "Nano-graphene in biomedicine: theranostic applications, Chem. Soc. Rev. **42**, 530 (2013).

[10] C.C. Berry and A.S.G. Curtis, "Functionalisation of magnetic nanoparticles for applications in biomedicine," J. Phys. D: Appl. Phys. **36**, R198 (2003).

[11] M. Mahmoudi, S. Sant, B. Wang, S. Laurent, and T. Sen, Advanced Drug Delivery Reviews **63**, (2011).

[12] P. Kucheryavy, J. He, V.T. John, P. Maharjan, L. Spinu, G.Z. Goloverda, and V.L. Kolesnichenko, "Superparamagnetic iron oxide nanoparticles with variable size and an iron oxidation state as prospective imaging agents," Langmuir **29**, 710 (2013).

[13] M. Talelli, C.J.F. Rijcken, T. Lammers, P.R. Seevinck, G. Storm, C.F. van Nostrum, and W.E. Hennink, "Superparamagnetic iron oxide nanoparticles encapsulated in biodegradable thermosensitive polymeric micelles: toward a targeted nanomedicine suitable for image-guided drug delivery," Langmuir **25**, 2060 (2009).

[14] D. Lee and J. Seo, "Magnetic frustration of graphite oxide," Sci Rep **7**, 44690 (2017).

[15] L. Babes, B. Denizot, G. Tanguy, J.J. Le Jeune, and P. Jallet, "Synthesis of Iron Oxide Nanoparticles Used as MRI Contrast Agents: A Parametric Study," Journal of Colloid and Interface Science **212**, 474 (1999).

[16] Z. Li, L. Wei, M.Y. Gao, and H. Lei, "One-Pot Reaction to Synthesize Biocompatible Magnetite Nanoparticles," Adv. Mater. **17**, 1001 (2005).

[17] Y. Zhao, J. Kang, and T. Tan, "Salt-, pH- and temperature-responsive semi-interpenetrating polymer network hydrogel based on poly(aspartic acid) and poly(acrylic acid)," Polymer **47**, 7702 (2006).

[18] A. Saha, S. Basiruddin, S.C. Ray, S.S. Roy, and N.R. Jana, "Functionalized graphene and graphene oxide solution *via* polyacrylate coating," Nanoscale **2**, 2777 (2010).

[19] J.-J. Lin, J.-S. Chen, S.-J. Huang, J.-H. Ko, Y.-M. Wang, T.-L. Chen, and L.-F. Wang, "Folic acid-Pluronic F127 magnetic nanoparticle clusters for combined targeting, diagnosis, and therapy applications," Biomaterials **30**, 5114 (2009).

[20] K. Yang, H. Gong, X. Shi, J. Wan, Y. Zhang, and Z. Liu, "In vivo biodistribution and toxicology of functionalized nano-graphene oxide in mice after oral and intraperitoneal administration," Biomaterials **34**, 2787 (2013).

[21] S. Roy, N. Soin, R. Bajpai, D.S. Misra, J.A. McLaughlin, and S.S. Roy, "Graphene oxide for electrochemical sensing applications," J. Mater. Chem. **21**, 14725 (2011).

[22] S. C. Ray, A. Saha, S. Basiruddin, S. Roy, and N.R. Jana, "Polyacrylate-coated graphene-oxide and graphene solution via chemical route for various biological application," Diamond and Related Materials **20**, 449 (2011).

[23] A. Ganguly, S. Sharma, P. Papakonstantinou, and J. Hamilton, "Probing the Thermal Deoxygenation of Graphene Oxide Using High-Resolution In Situ X-ray-Based Spectroscopies," J. Phys. Chem. C **115**, 17009 (2011).

[24] N. Soin, S.S. Roy, C. O'Kane, J.A.D. McLaughlin, T.H. Lim, and C.J.D. Hetherington, "Exploring the fundamental effects of deposition time on the microstructure of graphene nanoflakes by Raman scattering and X-ray diffraction," CrystEngComm **13**, 312 (2011).

[25] A.C. Ferrari and J. Robertson, "Origin of the 1150-cmÀ1 Raman mode in nanocrystalline diamond," Phys. Rev. B **63**, 121405 (2001).

[26] A. Kaniyoor and S. Ramaprabhu, "A Raman spectroscopic investigation of graphite oxide derived graphene," AIP Advances 2, 032183 (2012).

[27] R.E. Shroder, R.J. Nemanich, and J.T. Glass, "Analysis of the composite structures in diamond thin films by Raman spectroscopy," Phys. Rev. B **41**, 3738 (1990).

[28] N.B. Colthup, *Introduction to Infrared and Raman Spectroscopy* (New York, 1975).

[29] G. Consiglio, P. Di Pietro, L. D'Urso, G. Forte, G. Grasso, C. Sgarlata, D. Cossement, R. Snyders, and C. Satriano, "Surface tailoring of polyacrylate-grafted graphene oxide for controlled interactions at the biointerface," Journal of Colloid and Interface Science **506**, 532 (2017).

[30] D.C. Marcano, D.V. Kosynkin, J.M. Berlin, A. Sinitskii, Z. Sun, A. Slesarev, L.B. Alemany, W. Lu, and J.M. Tour, "Improved synthesis of graphene oxide," ACS Nano **4**, 4806 (2010).

[31] N. Soin, S.C. Ray, S. Sarma, D. Mazumder, S. Sharma, Y.-F. Wang, W.-F. Pong, S.S. Roy, and A.M. Strydom, "Tuning the Electronic and Magnetic Properties of NitrogenFunctionalized Few-Layered Graphene Nanoflakes," J. Phys. Chem. C **121**, 14073 (2017).

[32] C.-H. Chuang, S.C. Ray, D. Mazumder, S. Sharma, A. Ganguly, P. Papakonstantinou, J.-W. Chiou, H.-M. Tsai, H.-W. Shiu, and C.-H. Chen, "Chemical Modification of Graphene Oxide by Nitrogenation: An X-ray Absorption and Emission Spectroscopy Study," Sci Rep **7**, 42235 (2017).

[33] S.C. Ray, N. Soin, T. Makgato, C.H. Chuang, W.F. Pong, S.S. Roy, S.K. Ghosh, A.M. Strydom, and J.A. McLaughlin, "Graphene Supported Graphone/Graphane Bilayer Nanostructure Material for Spintronics," Sci Rep **4**, 3862 (2015).

[34] A. Hunt, D.A. Dikin, E.Z. Kurmaev, T.D. Boyko, P. Bazylewski, G.S. Chang, and A. Moewes, "Epoxide Speciation and Functional Group Distribution in Graphene Oxide Paper-Like Materials," Adv. Funct. Mater. **22**, 3950 (2012).

[35] D. Geng, S. Yang, Y. Zhang, J. Yang, J. Liu, R. Li, T.-K. Sham, X. Sun, S. Ye, and S. Knights, "Nitrogen doping effects on the structure of graphene," Applied Surface Science **257**, 9193 (2011).

[36] R.P. Gandhiraman, D. Nordlund, C. Javier, J.E. Koehne, B. Chen, and M. Meyyappan, "X-ray Absorption Study of Graphene Oxide and Transition Metal Oxide Nanocomposites," J. Phys. Chem. C **118**, 18706 (2014).

[37] D.O. Idisi, J.A. Oke, S. Sarma, S.J. Moloi, S.C. Ray, W.F. Pong, and A.M. Strydom, "Tuning of electronic and magnetic properties of multifunctional r-GO-ATA-Fe_2O_3-composites for magnetic resonance imaging (MRI) contrast agent," Journal of Applied Physics **126**, 035301 (2019).

[38] P.-G. Ren, D.-X. Yan, X. Ji, T. Chen, and Z.-M. Li, "Temperature dependence of graphene oxide reduced by hydrazine hydrate," Nanotechnology **22**, 055705 (2011).

[39] S.G. Urquhart and H. Ade, "Trends in the Carbonyl Core (C 1s, O 1s) $\rightarrow \pi^*_{C=O}$ Transition in the Near-Edge X-ray Absorption Fine Structure Spectra of Organic Molecules," J. Phys. Chem. B **106**, 8531 (2002).

[40] G. Tourillon, D. Guay, A. Fontaine, R. Garrett, and G.P. Williams, "Characterization of metal/organic molecule and metal/polymer interfaces by NEXAFS spectroscopy," Faraday Discuss. Chem. Soc. **89**, 275 (1990).

[41] J. Marco, J. Gancedo, M. Gracia, J. Gautier, E. Ríos, and F. Berry, "Characterization of the nickel cobaltite, $NiCo_2O_4$ prepared by several methods: An XRD, XANES, EXAFS, and XPS study," Journal of Solid State Chemistry **153**, 74 (2000).

[42] C. Viswanathan, V. Senthilkumar, R. Sriranjini, D. Mangalaraj, S.K. Narayandass, and J. Yi, Cryst, "Effect of substrate temperature on the properties of vacuum evaporated indium selenide thin films," Res. Technol. **40**, 658 (2005).

[43] G. Eda, G. Fanchini, M. Chhowalla, "Large-area ultrathin films of reduced graphene oxide as a transparent and flexible electronic material," Nature Nanotech. **3**, 270 (2008).

[44] D.S. Sutar, G. Singh, and V. Divakar Botcha, "Electronic structure of graphene oxide and reduced graphene oxide monolayers," Appl. Phys. Lett. **101**, 103103 (2012).

[45] G. Singh, V.D. Botcha, D.S. Sutar, P.K. Narayanam, S.S. Talwar, R.S. Srinivasa, and S.S. Major, "Near room temperature reduction of graphene oxide Langmuir–Blodgett monolayers by hydrogen plasma," Phys. Chem. Chem. Phys. **16**, 11708 (2014).

[46] M. Veerapandian, L. Zhang, K. Krishnamoorthy, and K. Yun, "Surface activation of graphene oxide nanosheets by ultraviolet irradiation for highly efficient anti-bacterials," Nanotechnology **24**, 395706 (2013).

[47] Y. Lin, Z. Feng, L. Yu, Q. Gu, S. Wu, and D.S. Su, "Insights into the surface chemistry and electronic properties of sp^2 and sp^3-hybridized nanocarbon materials for catalysis," Chem. Commun. **53**, 4834 (2017).

[48] O.V. Yazyev and L. Helm, "Defect-induced magnetism in graphene," Phys. Rev. B **75**, 125408 (2007).

[49] M.A.H. Vozmediano, M.P. López-Sancho, T. Stauber, and F. Guinea, "Local defects and ferromagnetism in graphene layers," Phys. Rev. B **72**, 155121 (2005).

[50] G. Li, A. Luican, J.M.B. Lopes dos Santos, A.H. Castro Neto, A. Reina, J. Kong, and E.Y. Andrei, "Observation of Van Hove singularities in twisted graphene layers," Nature Phys **6**, 109 (2010).

[51] M. Wang, W. Huang, M.B. Chan-Park, and C.M. Li, "Magnetism in oxidized graphenes with hydroxyl groups," Nanotechnology **22**, 105702 (2011).

[52] Y. Liu, N. Tang, X. Wan, Q. Feng, M. Li, Q. Xu, F. Liu, and Y. Du, "Realization of ferromagnetic graphene oxide with high magnetization by doping graphene oxide with nitrogen," Sci Rep **3**, 2566 (2013).

[53] K. Bagani, M.K. Ray, B. Satpati, N.R. Ray, M. Sardar, and S. Banerjee, "Contrasting Magnetic Properties of Thermally and Chemically Reduced Graphene Oxide," J. Phys. Chem. C **118**, 13254 (2014).

[54] A.Y.S. Eng, H.L. Poh, F. Šaněk, M. Maryško, S. Matějková, Z. Sofer, and M. Pumera, "Searching for magnetism in hydrogenated graphene," ACS Nano **7**, 5930 (2013).

[55] S. Qin, X. Guo, Y. Cao, Z. Ni, and Q. Xu, "Strong ferromagnetism of reduced graphene oxide," Carbon **78**, 559 (2014).

[56] T. Taniguchi, H. Yokoi, M. Nagamine, H. Tateishi, A. Funatsu, K. Hatakeyama, C. Ogata, M. Ichida, H. Ando, and M. Koinuma, "Correlated Optical and Magnetic Properties in Photoreduced Graphene Oxide," J. Phys. Chem. C **118**, 28258 (2014).

[57] M. Enayati, A. Nemati, A. Zarrabi, and M. A. Shokrgozar, "The role of oxygen defects in magnetic properties of gamma-irradiated reduced graphene oxide", *J. Alloy Comp.* **784**,134-148 (2019).

[58] M. Enayati, A. Nemati, A. Zarrabi and M.A. Shokrgozar, "Reduced Graphene Oxide: An Alternative for Magnetic Resonance Imaging Contrast Agent", *Mat. Lett.* **233**, 363-366 (2018).

[59] Z. He, X. Yang, H. Xia, X. Zhou, M. Zhao, Y. Song, and T. Wang, "Carbon nanonodules fewer than ten graphenes thick grown on aligned amorphous carbon nanofibers," Carbon **49**, 1939 (2011).

[60] Y. Ito, C. Christodoulou, M.V. Nardi, N. Koch, M. Kläui, H. Sachdev, and K. Müllen, "Tuning the Magnetic Properties of Carbon by Nitrogen Doping of Its Graphene Domains," J. Am. Chem. Soc. **137**, 7678 (2015).

[61] Q. Miao, L. Wang, Z. Liu, B. Wei, F. Xu, and W. Fei, "Magnetic properties of N-doped graphene with high Curie temperature," Sci Rep **6**, 21832 (2016).

[62] K.-C. Zhang, Y.-F. Li, Y. Liu, and Y. Zhu, "Density-functional study on the structural and magnetic properties of N-doped graphene oxide," Carbon **102**, 39 (2016).

[63] H. Araki and K. Yoshino, "Preparation, molecular structures and novel magnetic properties of organic ferromagnetic compounds by pyrolysis of triphenoxy-triazine and benzoguanamine," J. Phys.: Condens. Matter **4**, L119 (1992).

Figure captions:

Fig. 1: Transmission electron microscopy of (a) r-GO and (b) P-rGO samples. The XRD curves for the samples are shown in (c) and (d) deconvoluted Raman spectra showing the evolution of the D- and G-bands upon the polyacrylate grafting [Note: TEM of r-GO is taken from our previous report: *Microelectronic Engineering*, 146 (2015) 48-52].

Fig. 2: Deconvoluted core level x-ray photoelectron spectroscopy (XPS) spectra of (a) C 1s, (b) O 1s and (c) N 1s regions of the GO, r-GO, P-GO and P-rGO samples, (d) He-I ultraviolet photoelectron spectroscopy (UPS) of the samples shows with the highlighted lower kinetic energy part of UPS for estimation of work function and the higher kinetic energy for estimation of valence band maximum (VBM).

Fig. 3: X-ray absorption near edge structure (XANES) spectroscopy of the samples. (a) The deconvolution of the π^* region (shaded in grey) of (b) the corresponding C *K*-edge spectra. The (d) O *K*-edge and (f) N *K*-edge spectra of the samples is shown with their corresponding π^* region deconvolutions in (c, e), respectively.

Fig. 4: Linear current (I)–voltage (V) relationship for (a) GO, (c) r-GO and (e) P-rGO samples with the corresponding log (I)–(V) relationship shown in (b, d, f) respectively. (g) Magnetization (M) *vs* applied magnetic field (H) loops obtained at a temperature of 2 K and (h) magnetization (M) *vs* temperature (T) curve obtained at an applied field of 500 Oe.

Table 1: Elemental composition and quantification from XPS analysis; Raman spectra peak analysis; Valence Band Maximum (VBM) and maximum magnetisation (M_{MAX}), coercivity (H_C) parameters for the samples.

	XPS analysis					**Raman**	**XANES**	**XRD**	**He-I UPS**	**Magnetisation**
	C 1s (at%)	O 1s (at%)	N 1s (at%)	S 2p (at%)	P 2p (at %)	I_D/I_G	π* (a.u.)	d-spacing (nm)	VBM (eV)	M_S @2K (emu/g) x 10^{-3}
GO	56.9	43.1	-	-	-	1.12	2.76	0.702	-	4.56
r-GO	81.0	17.9	1.1	-	-	1.06	2.29	0.374	4.0	5.61
P-GO	68.0	30.3	0.5	1.0	0.2	1.15	1.25	0.408	4.1	5.55
P-rGO	77.0	20.0	1.9	0.7	0.4	1.35	2.05	0.381	4.2	9.56

Table 2: Deconvolution parameters including the peak position, intensity and FWHM for the C *K*-edge XANES spectra of the samples.

	Peak-I			Peak-II			Peak-III			Peak-IV			Peak-V		
	Pos. (eV)	Δω (eV)	Int. (a.u.)	Pos. (eV)	Δω (eV)	Int. (a.u.)	Pos. (eV)	Δω (eV)	Int. (a.u.)	Pos. (eV)	Δω (eV)	Int. (a.u.)	Pos. (eV)	Δω (eV)	Int. (a.u.)
GO	283.6	1.20	0.36	285.0	0.98	0.16	285.6	1.63	0.65	287.8	1.55	0.35	290.0	0.73	0.02
r-GO	283.2	1.46	0.38	284.7	1.18	0.33	285.7	1.90	0.46	287.5	1.32	0.13	-	-	-
P-GO	284.2	1.69	0.14	285.3	1.17	0.12	286.5	1.01	0.16	287.3	2.15	0.24	288.71	1.54	0.03
P-rGO	284.5	1.76	0.46	285.3	0.98	0.10	286.3	1.07	0.23	287.3	1.83	0.53	288.7	1.46	0.12

Table 3: Deconvolution parameters including the peak position, intensity and FWHM for the O K-edge and N K-edge XANES spectra of the samples.

	O *K*-edge XANES									**N *K*-edge XANES**								
	Peak-I			Peak-II			Peak-III			Peak-I			Peak-II			Peak-III		
	x1 (eV)	Δω (eV)	Int. (a.u.)	x2 (eV)	Δω (eV)	Int. (a.u.)	x3 (eV)	Δω (eV)	Int. (a.u.)	x1 (eV)	Δω (eV)	Int. (a.u.)	x2 (eV)	Δω (eV)	Int. (a.u.)	x3 (eV)	Δω (eV)	Int. (a.u.)
GO	528.9	1.40	0.02	529.6	0.98	0.02	-	-	-	-	-	-	-	-	-	-	-	-
r-GO	528.2	1.82	0.03	528.9	1.40	0.02	529.7	0.83	0.01	398.9	1.44	0.03	399.8	0.85	0.01	-	-	-
P-GO	-	-	-	529.9	1.83	0.02	530.7	1.46	0.03	399.3	1.50	0.02	400.2	0.91	0.02	-	-	-
P-rGO	-	-	-	530.0	1.58	0.04	530.7	1.25	0.03	398.4	1.03	0.04	397.5	0.49	0.01	397.1	1.3	0.01

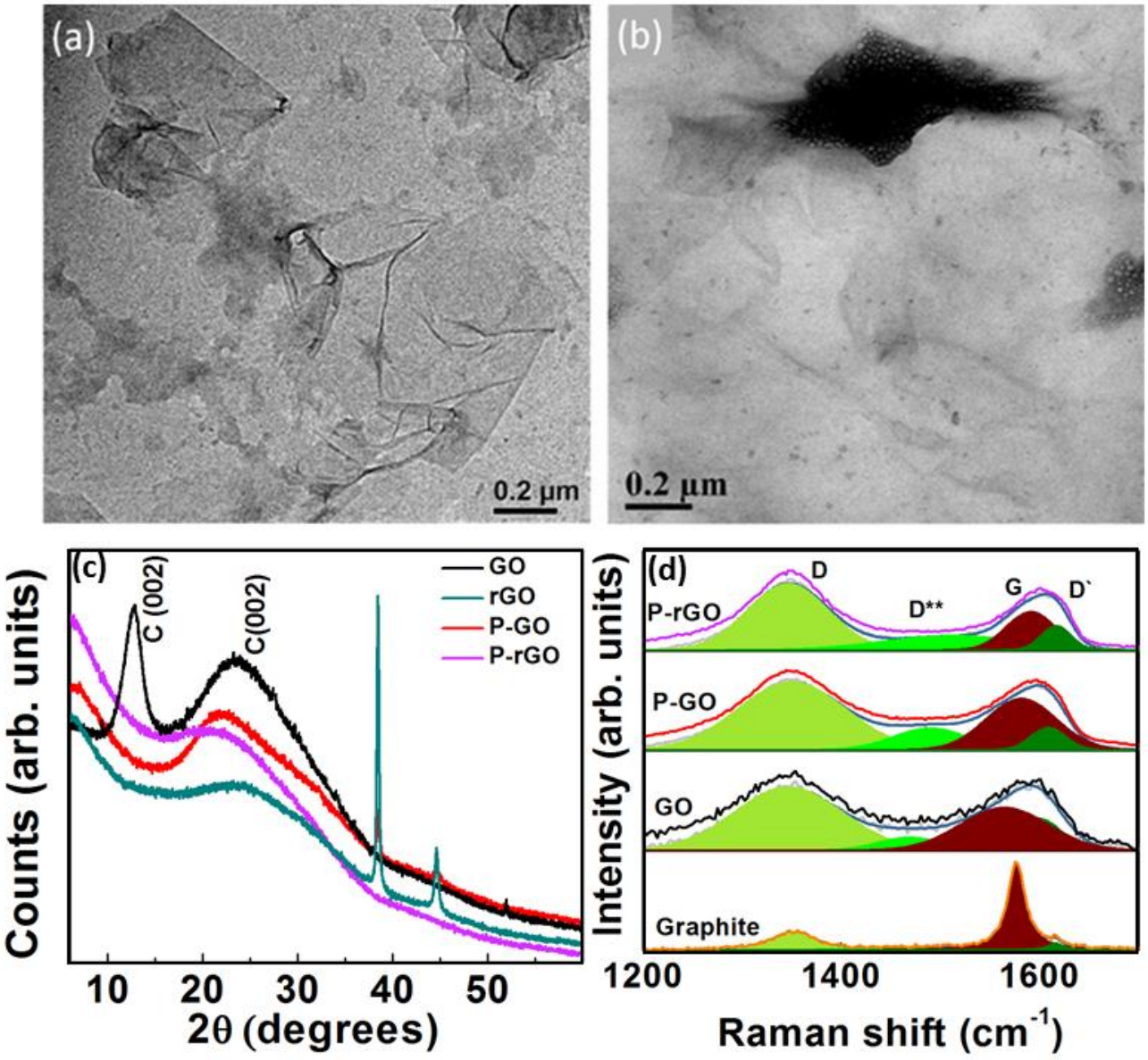
(a)
0.2 µm
(b)
0.2 µm
(c)
C (002)
C(002)
GO
rGO
P-GO
P-rGO
Counts (arb. units)
10
20
30
40
50
2θ (degrees)
(d)
D
D**
G
D`
P-rGO
P-GO
GO
Graphite
Intensity (arb. units)
1200
1400
1600
Raman shift (cm-1)

Fig. 1

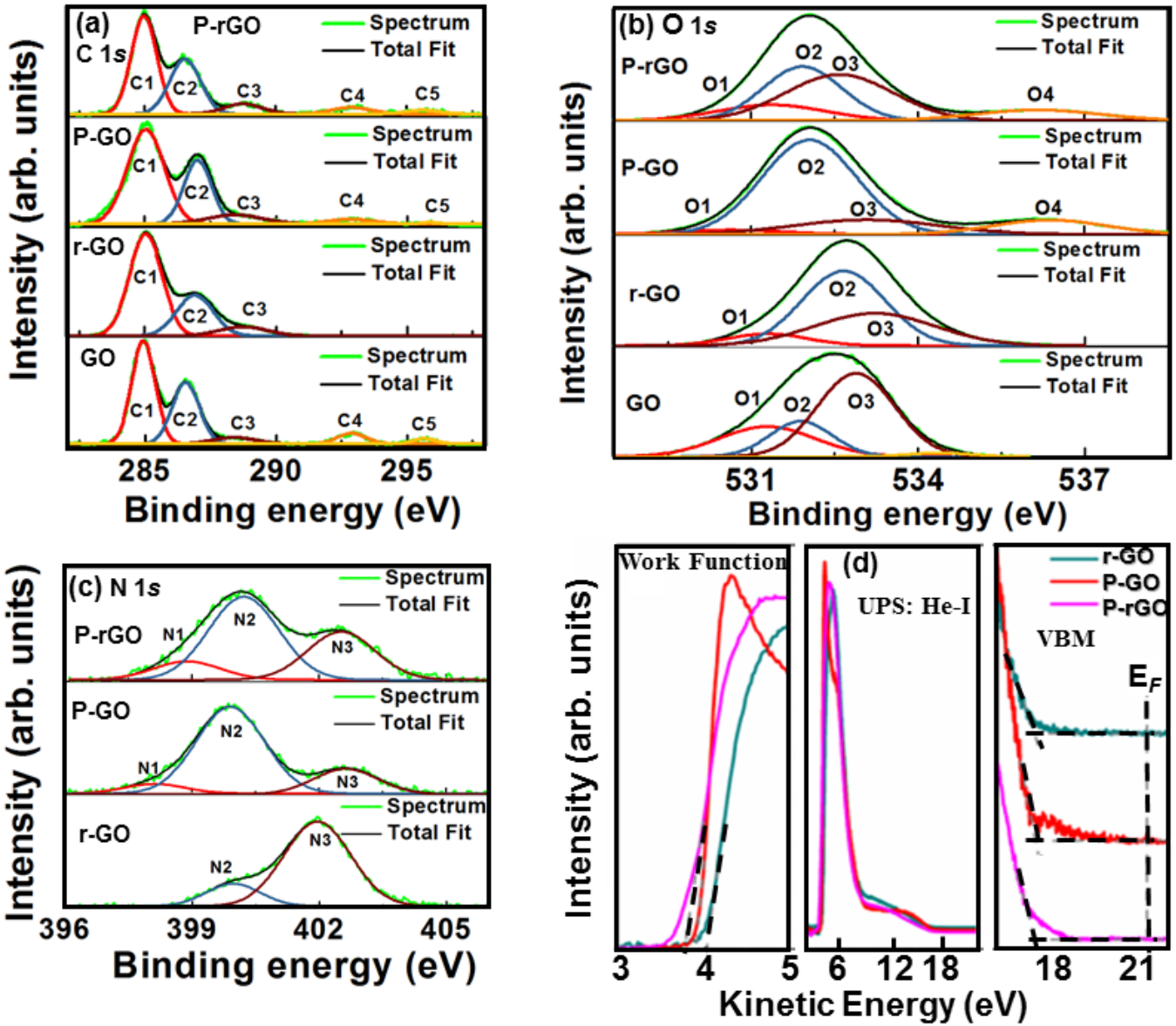
(a)
C 1s
P-rGO
P-GO
r-GO
GO
Spectrum
Total Fit
C1
C2
C3
C4
C5
Intensity (arb. units)
285
290
295
Binding energy (eV)
(b) O 1s
O1
O2
O3
O4
531
534
537
(c) N 1s
N1
N2
N3
396
399
402
405
Work Function
(d)
UPS: He-I
VBM
E_F
r-GO
P-GO
P-rGO
3
4
5
6
12
18
21
Kinetic Energy (eV)

Fig. 2

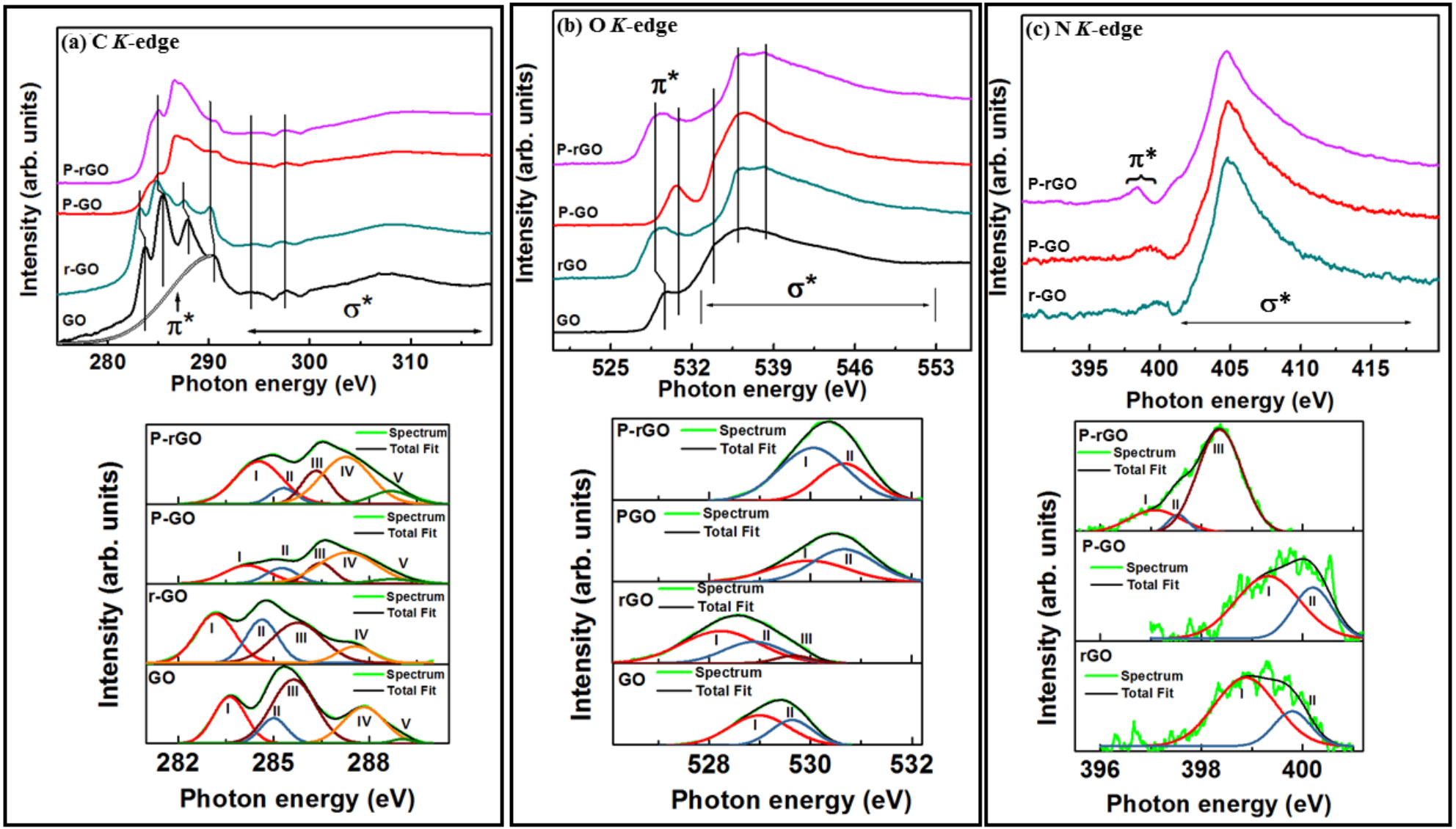
(a) C K-edge
Intensity (arb. units)
P-rGO
P-GO
r-GO
GO
π*
σ*
280
290
300
310
Photon energy (eV)
Spectrum
Total Fit
I
II
III
IV
V
282
285
288
(b) O K-edge
rGO
525
532
539
546
553
PGO
528
530
532
(c) N K-edge
395
400
405
410
415
396
398
400

Fig. 3

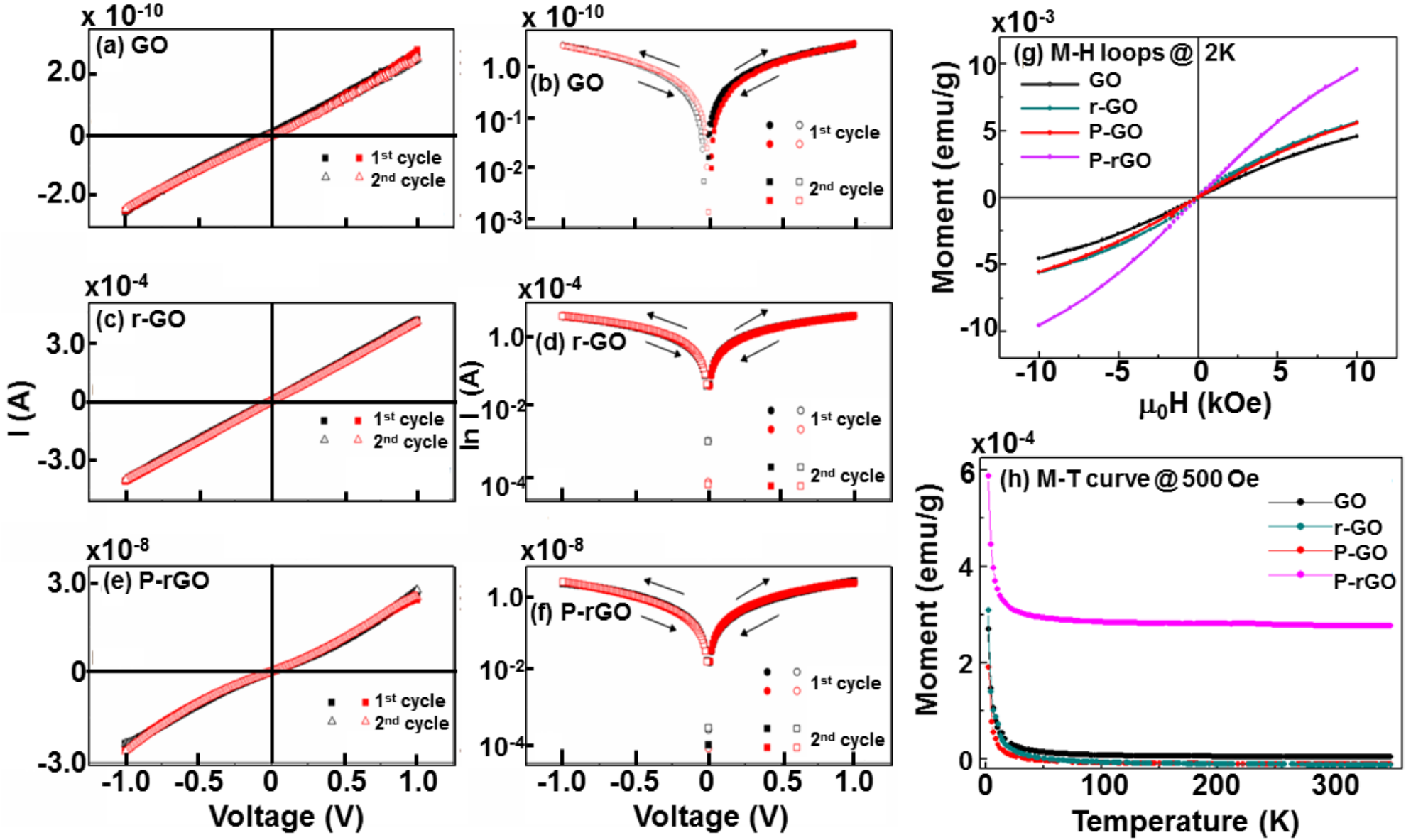
x 10-10
(a) GO
2.0
0
-2.0
1st cycle
2nd cycle
x 10-10
(b) GO
1.0
10-1
10-2
10-3
1st cycle
2nd cycle
x10-3
(g) M-H loops @ 2K
GO
r-GO
P-GO
P-rGO
Moment (emu/g)
10
5
0
-5
-10
-10
-5
0
5
10
μ0H (kOe)
x10-4
(c) r-GO
3.0
0
-3.0
I (A)
1st cycle
2nd cycle
x10-4
(d) r-GO
1.0
10-2
10-4
ln I (A)
1st cycle
2nd cycle
x10-4
(h) M-T curve @ 500 Oe
GO
r-GO
P-GO
P-rGO
Moment (emu/g)
6
4
2
0
0
100
200
300
Temperature (K)
x10-8
(e) P-rGO
3.0
0
-3.0
1st cycle
2nd cycle
x10-8
(f) P-rGO
1.0
10-2
10-4
1st cycle
2nd cycle
-1.0
-0.5
0
0.5
1.0
Voltage (V)
-1.0
-0.5
0
0.5
1.0
Voltage (V)

Fig. 4